Available online at www.sciencedirect.com

ScienceDirect

Energy Procedia 161 (2019) 446–453

Energy Procedia

www.elsevier.com/locate/procedia

2nd International Conference on Sustainable Energy and Resource Use in Food Chains, ICSEF 2018, 17-19 October 2019, Paphos, Cyprus

Effect of cross-section geometry on the thermohydraulic characteristics of supercritical CO_2 in minichannels

Lei Chai* and Savvas A Tassou

Brunel University London, Institute of Energy Futures, RCUK Centre for Sustainable Energy use in Food chains (CSEF), Uxbridge, UB8 3PH, United Kingdom

Abstract

Carbon dioxide (CO_2) is becoming an important commercial and industrial working fluid as a potential replacement of the non-environmental friendly refrigerants. For refrigeration and power systems, the minichannel heat exchangers are becoming attractive for transcritical CO_2 Rankine cycle and supercritical CO_2 Brayton cycle, due to their highly compact construction, high heat transfer coefficient, high pressure capability and lower fluid inventory. This paper employs three-dimensional numerical models to investigate the heat transfer and pressure drop characteristics of supercritical CO_2 in minichannels. The models consider real gas thermophysical properties and buoyancy effect and investigate the effect of cross-section geometry on the thermohydraulic characteristics. Six minichannel cross-section geometries with the same hydraulic diameter of 1.22 mm are considered. The geometries include circle, semicircle, square, equilateral triangle, rectangle (aspect ratio = 2) and ellipse (aspect ratio = 2). The inlet temperature, outlet pressure and wall heat flux are 35 °C/75 bar/100 kW/m^2 and 35 °C/150 bar/300 kW/m^2 for heating conditions and 120 °C/75 bar/-100 kW/m^2 and 120 °C/150 bar/-300 kW/m^2 for cooling conditions. Comparisons of local Nusselt number and friction factor with those employed empirical correlations are made and useful information and guidelines are provided for the design of compact heat exchangers for supercritical CO_2 power system applications.

Selection and peer-review under responsibility of the 2nd International Conference on Sustainable Energy and Resource Use in Food Chains, ICSEF2018

Keywords: Numerical simulation; thermohydraulic characteristic; supercritical CO_2; cross-section geometry; minichannel;

* Corresponding author. Tel.: +44-189-526-5834.
E-mail address: Lei.Chai@brunel.ac.uk

Selection and peer-review under responsibility of the 2nd International Conference on Sustainable Energy and Resource Use in Food Chains, ICSEF2018.
10.1016/j.egypro.2019.02.077

Nomenclature

D	hydraulic diameter, m	Greek letters	
f	friction factor	ρ	density, kg/m^3
h	heat transfer coefficient, W/(m^2·K)	λ	thermal conductivity, W/(m·K)
L	length, m	μ	dynamic viscosity, Pa·s
Nu	Nusselt number	*Subscripts*	
p	pressure, Pa	in	inlet
q	heat flux, W/m^2	f	fluid, fiction
Re	Reynolds number	out	outlet
T	temperature, K	z	local
u	velocity, m/s[1]		

1. Introduction

Carbon dioxide (CO_2) in refrigeration and heat pump systems has a zero net impact on climate change and reduces the emission of greenhouse gas [1]. These attributes have made it gain increased attentions among researchers and become a potential replacement for the non-environmental friendly refrigerants such as chlorofluoro-carbon (CFC) and hydro-chlorofluorocarbons (HCFC). Furthermore, supercritical CO_2 Brayton cycle has recently been developed for power generation and conversion system. Due to its operation at high pressures throughout the cycle, supercritical CO_2 can have a higher power density and lead to reduced pumping/compression power, smaller equipment sizes, smaller plant footprint, and thus improved efficiency in power cycle and lower capital cost [2].

In the refrigeration, heat pump and power generation systems, heat exchanger is the key component in transferring the thermal energy, which can be used as the heater, cooler, evaporator, condenser and recuperator. Among the various types of heat exchangers, the minichannel heat exchanger (arbitrarily defined here as channels with a hydraulic diameter of 0.2 mm to 3 mm, Kandlikar and Grande [3]) has been preferably applied due to its highly compact construction, high heat transfer coefficient, high pressure capability and lower fluid inventory. To the authors' knowledge, most of the existing work on the thermohydraulic characteristics of supercritical CO_2 has been carried out on circle or semi-circle channels. However, minichannel heat exchanger with different cross-section geometries are being manufactured in recent years, and the cross-section geometry shows significant influence on fluid flow and heat transfer characteristics [4]. Furthermore, as a result of the significant variation of thermophysical properties of CO_2 in the near-critical point region, the heat transfer characteristics are quite different from those with constant physical properties, and the heat transfer efficiency changes considerably depending on flow conditions. For a detailed understanding into the thermohydraulic characteristics of supercritical CO_2 in minichannels, three-dimensional numerical models with NIST real gas thermophysical properties and buoyancy effect are developed and six different cross-section geometries are examined under both heating and cooling conditions.

2. Computational method

In order to examine the effect of cross-section geometry on thermohydraulic characteristics of supercritical CO_2, six different cross-section geometries, including circle, semicircle, square, equilateral triangle, rectangle (aspect ratio = 2) and ellipse (aspect ratio = 2) are designed in the present work as shown in Fig. 1. These cross-section geometries have the same hydraulic diameter of 1.22 mm and the same channel length of 248 mm. Supercritical CO_2 flows in the channels under heating or cooling conditions. The NIST real gas thermophysical properties and buoyancy effect are included in the computational models. The standard k-ε model is adopted for the turbulent simulation.

The present work implements the software ANSYS Fluent 17.0 and incorporates the REFPROP v9.1 for numerical calculation. Velocity-inlet with constant temperature and pressure-outlet boundary conditions are respectively employed in the channel inlet and outlet. Constant wall heat flux is adopted to the channel wall. For these studies, we focus on the supercritical CO_2 temperature range from 35 to 120 °C, and keep the similar heat flux values for the same outlet pressure condition. Four different boundaries for heating and cooling conditions are selected and listed in Table 1. The corresponding mass flux for the four cases are 545.6, 1629.5, 473.9 and 561.3 kg/(m^2·s), respectively. The SIMPLEC algorithm is used to solve the governing differential equations for the velocity, pressure and temperature

fields in the control volume. The convergence criteria are less than 10^{-5} for the normalised residuals of all variables in momentum and energy equations. A grid independence test is checked using several different mesh sizes. A total number of generated meshes about 0.670 million, 0.900 million, 0.776 million, 1.828 million, 0.896 million and 0.856 million is applied for the channels respectively with circle, semicircle, square, equilateral triangle, rectangle and ellipse cross-section geometries.

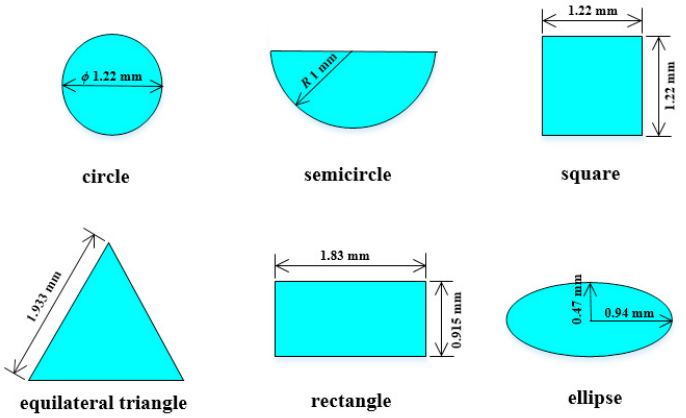

Fig. 1. Different cross-section geometries of analysis model.

Table 1 Boundary conditions for different operating conditions.

Case	T_{in} (°C)	u_{in} (m/s)	q (kW/m^2)	p_{out} (bar)
#1	35	2	100	75
#2	35	2	300	150
#3	120	4	-100	75
#4	120	2	-300	150

3. Data acquisition

The parameters relevant to the thermohydraulic characteristics are indicated in Table 2.

Table 2. Parameters relevant to the local and average thermohydraulic characteristics.

Local thermohydraulic parameters		Average thermohydraulic parameters	
$Re_z = \frac{GD}{\mu_z}$	(1)	$\overline{Re} = \frac{\int_0^L Re_z dz}{L}$	(5)
$h_z = \frac{q_z}{T_{w,z} - T_{f,z}}$	(2)	$\overline{h} = \frac{\int_0^L h_z dz}{L}$	(6)
$Nu_z = \frac{h_z D}{\lambda_{f,z}}$	(3)	$\overline{Nu} = \frac{\int_0^L Nu_z dz}{L}$	(7)
$f_z = \frac{2\rho_z D}{G^2}\frac{dp_f}{dz}$	(4)	$\overline{f} = \frac{\int_0^L f_z dz}{L}$	(8)

* G: mass flux; D: hydraulic diameter; q_z: local heat flux; $T_{w,z}$: local wall temperature, $T_{f,z}$: local fluid temperature; ρ_z: local density; μ_z: local dynamic viscosity; $\lambda_{f,z}$: local thermal conductivity; dp_f/dz: pressure gradient due to the friction; L: channel length.

4. Results and discussion

4.1. Thermohydraulic characteristics

Figure. 2 shows the local temperature of supercritical CO_2 along the flow direction. For different boundary conditions, the local temperatures present different patterns due to the significant variation of thermophysical properties. For the different cross-section geometries, the local temperatures display little difference between each other due to the little difference in the ratio of heat transfer rate to the fluid inventory. It can be seen that for the same boundary condition, the circle and ellipse channels show the maximum temperature change while the triangle one shows minimum change.

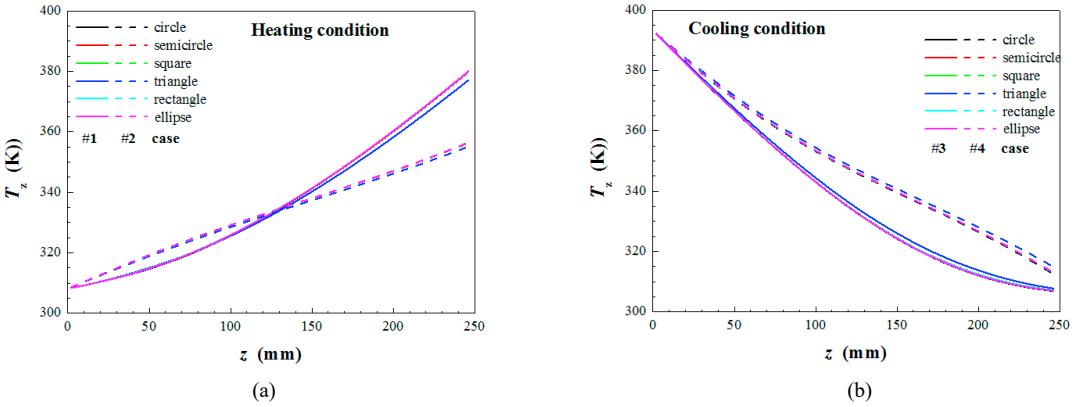

Fig. 2. Local fluid temperature: (a) Heating condition. (b) Cooling condition.

Figure. 3 shows the local heat transfer coefficients for both heating and cooling conditions. Higher heat transfer coefficients are found at the channel inlets due to the entrance effect. Different boundary conditions result in different pattern of local heat transfer coefficient, mainly caused by the different fluid mass flux and varied thermophysical properties. For the heating conditions, the results with boundary cases #1 (from Table 1) drop quickly and then keep steady with a slow decrease along the flow direction, while the results with boundary cases #2 drop at a more slower rate or even rise a little after the entrance effect, because they cover the pseudocritical point region. For the cooling conditions with boundary cases #3, the rate of heat transfer significantly increases towards the near-critical point, while for boundary cases #4, it increases slowly in the near pseudocritical point region and decreases slowly after that. For the same boundary condition, the circle and ellipse channels present the highest local heat transfer coefficient, the semicircle, rectangle and square ones follow, and the triangle one shows the lowest, except in the region $z > 100$ mm for boundary cases #3, where the wall temperature starts to go below the critical temperature (31.1 °C).

Figure. 4 shows the corresponding local Nusselt numbers. As the definition, Nusselt number is determined by the heat transfer coefficient and thermal conductivity of fluid. With the increase of fluid temperature and away from the critical point, the thermal conductivity of supercritical CO_2 drops quickly and then keep steady, and the decrease rate becomes slower with increased pressure. Therefore, after the entrance effect, the local Nusselt numbers for boundary cases #1 decrease very slowly and those for boundary cases #2 even increase along the flow direction. For boundary cases #3, the increase rate of local Nusselt numbers becomes lower than that of local heat transfer coefficient, and for boundary cases #4, the local Nusselt numbers increase a little and then decrease along the flow direction.

Figure. 5 shows the local pressure drop for both heating and cooling conditions. It can be seen that for a fixed z position and under the same boundary condition, the circle and ellipse channels shows the maximum pressure drop, the semicircle, rectangle and square ones follows, and the triangle one shows the minimum.

Figure. 6 shows the corresponding local friction factor. After the entrance effect, the local friction factors keep steady along the flow direction for channels with boundary cases #1 and #2, while the local friction factors for boundary case #3 climb up after $z > 100$ mm and those for boundary case #4 climb down along the flow direction.

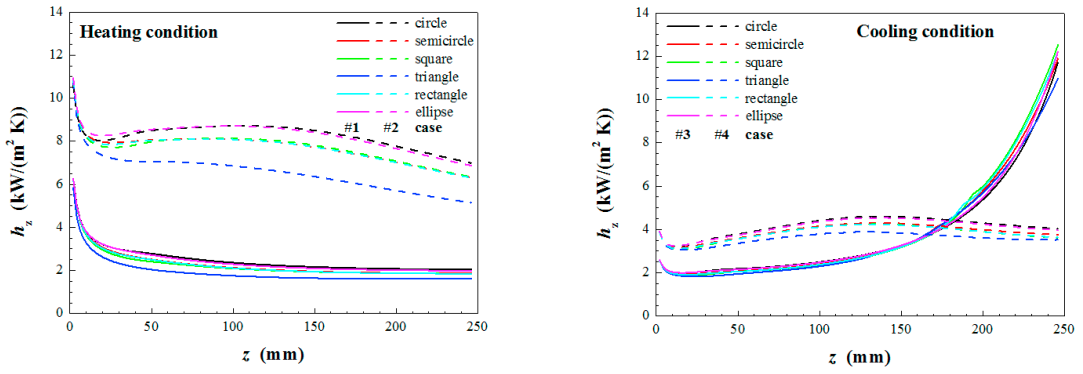

(a) (b)

Fig. 3. Local heat transfer coefficient: (a) Heating condition. (b) Cooling condition.

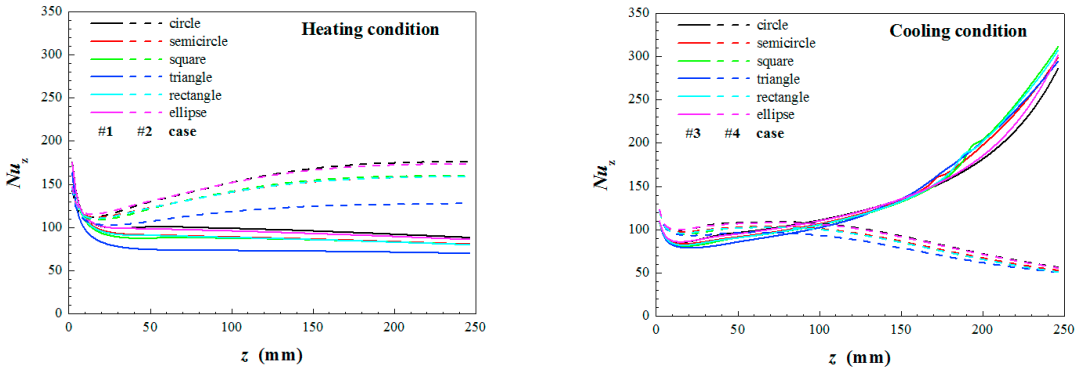

(a) (b)

Fig. 4. Local Nusselt number: (a) Heating condition. (b) Cooling condition.

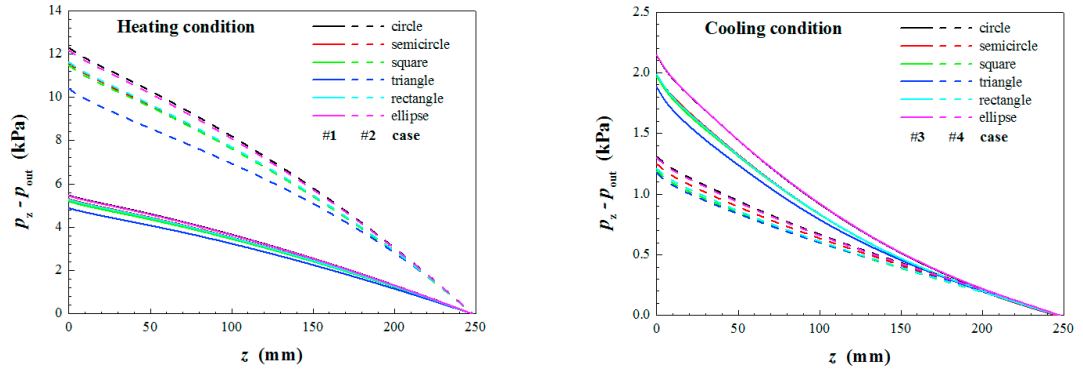

(a) (b)

Fig. 5. Local pressure drop: (a) Heating condition. (b) Cooling condition.

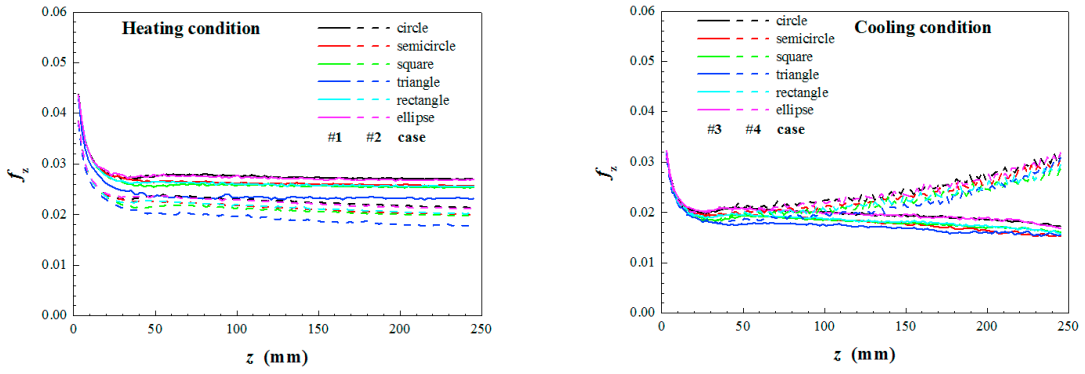

Fig. 6. Local friction factor: (a) Heating condition. (b) Cooling condition.

To directly demonstrate the effect of cross-section geometry on thermohydraulic characteristics of supercritical CO_2 in minichannels, Table 3 lists the computational fluid dynamics (CFD) results of average thermohydraulic characteristics, including $\overline{Re}$, $\overline{Nu}$ and $\overline{f}$.

Table 3 CFD results of average thermohydraulic characteristics.

Geometry	Case	$\overline{Re}$	$\overline{Nu}$	$\overline{f}$
circle	#1	33276	98.9	0.0280
	#2	44165	154.0	0.0231
	#3	285801	139.9	0.0199
	#4	18742	92.4	0.0243
semicircle	#1	33284	90.5	0.0268
	#2	44118	142.6	0.0220
	#3	28622	142.7	0.0183
	#4	18806	87.5	0.0233
square	#1	33283	88.9	0.0264
	#2	44161	142.9	0.0215
	#3	28607	143.6	0.0185
	#4	18793	86.0	0.0224
triangle	#1	33311	76.6	0.0243
	#2	43624	119.6	0.0199
	#3	28727	141.6	0.0175
	#4	19036	81.6	0.0219
rectangle	#1	33281	89.9	0.0266
	#2	44151	142.3	0.0221
	#3	28620	143.5	0.0187
	#4	18800	86.2	0.0226
ellipse	#1	33276	96.6	0.0278
	#2	44174.	153.4	0.0229
	#3	28591	141.8	0.0199
	#4	18799	91.7	0.0240

4.2. Comparison with empirical correlations

Six empirical correlations of Nusselt number are selected to compare the CFD heat transfer results. Three of them are the traditional heat transfer correlations for turbulent flow in circular tubes, including Dittus-Boelter correlation [5], Sieder and Tate correlation [6] and Gnielinski correlation [7], and the other three are particular for heat transfer of supercritical CO_2 in horizontal tubes, including Krasnoshchekov and Protopopov correlation [8], Pitla et al. correlation [9] and Dang and Hihara correlation [10]. As shown in Fig. 7, the Krasnoshchekov and Protopopov

correlation shows the best prediction for the heating conditions, with the difference less than 5% after the entrance effect. For the cooling condition #4, the Krasnoshchekov and Protopopov correlation also predicts well, with the difference less than 8% after the entrance effect. For the cooling condition #3, there is no empirical correlation good enough to predict the CFD result, in particular for the region with the wall temperature lower than the critical point.

Two empirical correlations of friction factor (shown in Table 3) for turbulent flow in circular tubes, including Blasius correlation and Petukhov correlation [11], are used to compare the CFD results. As shown in Fig. 8, these two correlations can predict the friction factor well for boundary cases #2 with a difference of less than 7%, while under predicts by 16-18% of the CFD results for the boundary cases #1. Both of the two correlations overpredict the CFD results for cooling conditions, 15-43% higher for the boundary cases #3 and 0-15% higher for the boundary cases #4.

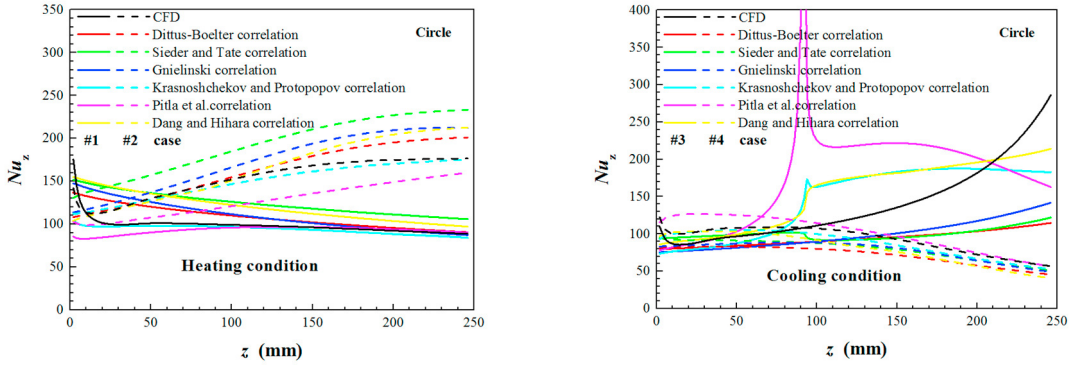

Fig. 7. Comparison of local Nusselt number with empirical correlations: (a) Heating condition. (b) Cooling condition.

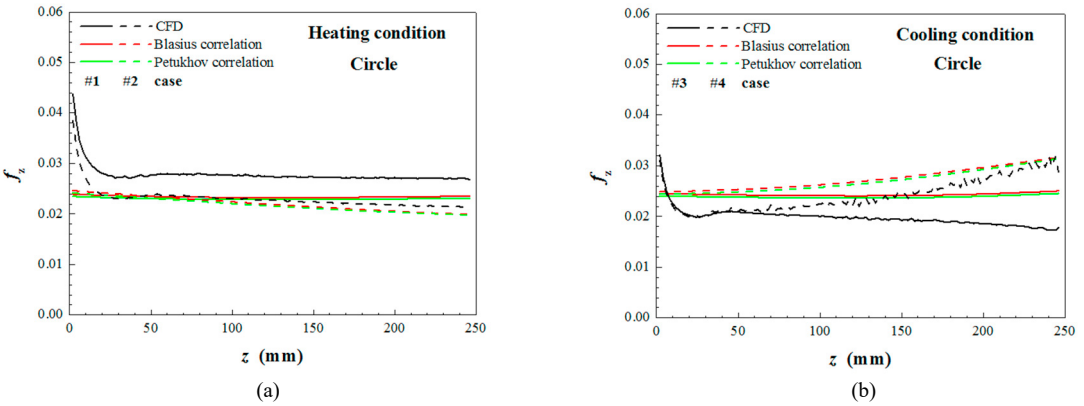

Fig. 8. Comparison of local friction factor with empirical correlations: (a) Heating condition. (b) Cooling condition.

5. Conclusions

The effect of cross-section geometry on thermohydraulic characteristics of supercritical CO2 in mimichannels was examined with the three dimensional model developed Local and average thermohydraulic characteristics are investigated and compared with the empirical correlations under both heating and cooling conditions. Based on the CFD results, the following conclusions can be drawn.

Different boundary conditions lead to significantly different patterns of local and average thermohydraulic characteristics. Different cross-section geometries under the same boundary conditions clearly result in different local and average heat transfer and pressure drop. Larger heat transfer coefficient is usually accompanied by larger pressure drop. As the channel wall temperature is higher than the critical point, the circle and ellipse channels have the highest

heat transfer coefficient, followed by the semicircle, rectangle and square ones, and the triangle cross-section has the lowest. Krasnoshchekov and Protopopov correlation can predict the CFD heat transfer results well, with the difference less than 5% for the heating conditions, and less than 8% for the cooling conditions with wall temperature higher than the critical point. For the cooling condition with wall temperature lower than the critical point, all the tested six empirical correlations fail to predict the heat transfer results. For heating conditions, Blasius correlation and Petukhov correlation predict the friction factor well for the case with 150 bar outlet pressure, and underpredict 16-18% for the case with 75 bar outlet pressure. For the cooling conditions, both of them overpredict the CFD results, 15-43% higher for the cases with 75 bar outlet pressure and 0-15% higher for the cases with 150 bar outlet pressure.

Acknowledgements

The work presented in this paper is supported by a number of funders as follows: i) The Engineering and Physical Sciences Research Council (EPSRC) of the UK under research grants EP/P004636/1 'Optimising Energy Management in Industry - OPTEMIN', and EP/K011820/1 (Centre for Sustainable Energy Use in Food Chains) and ii) the European Union's Horizon 2020 research and innovation programme under grant agreement No. 680599. The authors would like to acknowledge the financial support received by the project funders and the industry partners.

References

[1] Austin B T, Sumathy K. Transcritical carbon dioxide heat pump systems: A review. *Renewable and Sustainable Energy Reviews*, 2011, 15(8): 4013-4029.
[2] Fundamentals and applications of supercritical carbon dioxide (sCO_2) based power cycles. Woodhead Publishing, 2017.
[3] S.G. Kandlikar, W.J. Grande, Evolution of microchannel flow passages – thermohydraulic performance and fabrication technology. *Heat Transfer Engineering*, 24 (2003) 3-17.
[4] Kandlikar S, Garimella S, Li D, et al. Heat transfer and fluid flow in minichannels and microchannels, Elsevier, 2005.
[5] Winterton R H S. Where did the Dittus and Boelter equation come from?. *International Journal of Heat and Mass Transfer*, 1998, 41(4-5): 809-810.
[6] Sieder E N, Tate G E. Heat transfer and pressure drop of liquids in tubes. *Industrial & Engineering Chemistry*, 1936, 28(12): 1429-1435.
[7] Gnielinski V. New equations for heat and mass transfer in turbulent pipe and channel flow. *International Chemical Engineering*, 1976, 16(2): 359-368.
[8] Krasnoshchekov E A, Protopopov V S. Experimental study of heat exchange in carbon dioxide in the supercritical range at high temperature drops (Heat transfer in turbulent carbon dioxide pipeflow at supercritical region). *High Temperature*, 1966, 4: 375-382.
[9] Pitla S S, Groll E A, Ramadhyani S. New correlation to predict the heat transfer coefficient during in-tube cooling of turbulent supercritical CO_2. *International Journal of Refrigeration*, 2002, 25(7): 887-895.
[10] Dang C, Hihara E. In-tube cooling heat transfer of supercritical carbon dioxide. Part 1. Experimental measurement. *International Journal of Refrigeration*, 2004, 27(7): 736-747.
[11] Petukhov B S, Kirillov P L. About heat transfer at turbulent fluid flow in tubes. *Thermal Engineering*, 1958, 4: 63-68.